J. Fluid Mech. (2024), *vol*. 984, R3, doi:10.1017/jfm.2024.206

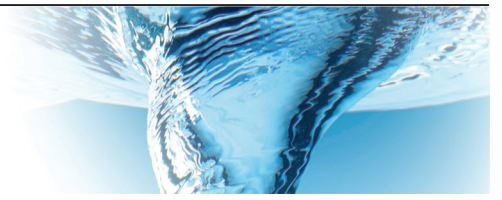

Numerical study on the mechanism of drag modulation by dispersed drops in two-phase Taylor–Couette turbulence

Jinghong Su[1], Lei Yi[1], Bidan Zhao[2], Cheng Wang[1], Fan Xu[2], Junwu Wang[2,4,†] and Chao Sun[1,3,†]

[1]New Cornerstone Science Laboratory, Center for Combustion Energy, Key Laboratory for Thermal Science and Power Engineering of Ministry of Education, Department of Energy and Power Engineering, Tsinghua University, 100084 Beijing, PR China

[2]State Key Laboratory of Multiphase Complex Systems, Institute of Process Engineering, Chinese Academy of Sciences, P.O. Box 353, 100190 Beijing, PR China

[3]Department of Engineering Mechanics, School of Aerospace Engineering, Tsinghua University, 100084 Beijing, PR China

[4]College of Mechanical and Transportation Engineering, China University of Petroleum, 102249 Beijing, PR China

(Received 1 December 2023; revised 22 January 2024; accepted 18 February 2024)

The presence of a dispersed phase can significantly modulate the drag in turbulent systems. We derived a conserved quantity that characterizes the radial transport of azimuthal momentum in the fluid–fluid two-phase Taylor–Couette turbulence. This quantity consists of contributions from advection, diffusion and two-phase interface, which are closely related to density, viscosity and interfacial tension, respectively. We found from interface-resolved direct numerical simulations that the presence of the two-phase interface consistently produces a positive contribution to the momentum transport and leads to drag enhancement, while decreasing the density and viscosity ratios of the dispersed phase to the continuous phase reduces the contribution of local advection and diffusion terms to the momentum transport, respectively, resulting in drag reduction. Therefore, we concluded that the decreased density ratio and the decreased viscosity ratio work together to compete with the presence of a two-phase interface for achieving drag modulation in fluid–fluid two-phase turbulence.

Key words: drag reduction, turbulence simulation, multiphase flow

† Email addresses for correspondence: jwwang@cup.edu.cn, chaosun@tsinghua.edu.cn

1. Introduction

Two-phase flow, consisting of two immiscible fluids, is widely encountered in various engineering applications. The presence of a dispersed phase can significantly alter the flow characteristics, leading to either drag enhancement or drag reduction (Balachandar & Eaton 2010; Ceccio 2010; Lohse 2018; Mathai, Lohse & Sun 2020; Yi *et al.* 2023). A correct understanding of the mechanism of drag modulation is of great significance to relevant engineering applications; however, a comprehensive understanding of this mechanism is still missing.

A typical characteristic of liquid–liquid two-phase flow is the dynamics of the interface, which involves deformation (Rallison 1984; Rosti, De Vita & Brandt 2019; Hakansson *et al.* 2022), coalescence (Stone 1994; Kavehpour 2015) and breakup (Lemenand *et al.* 2017; Olad *et al.* 2023; Ni 2024). When coalescence is counterbalanced by breakup, the dispersed phase exhibits a specific size distribution which can be well described by a lognormal distribution (Yi, Toschi & Sun 2021). Under fixed Reynolds number, the dispersed phase has almost the same average size for different volume fractions (Yi *et al.* 2022). It has been observed that the dispersed phase volume fraction is positively correlated with the global transport of a liquid–liquid two-phase turbulent flow (Yi *et al.* 2022), indicating that increasing the interfacial area could contribute to the drag enhancement. The effect of dispersed phase coalescence in liquid–liquid two-phase flow has recently been studied using interface-resolved direct numerical simulations (De Vita *et al.* 2019; Cannon *et al.* 2021), and it is found that the coalescence effectively decreases the interfacial area, thus weakening the drag enhancement effect, and vice versa (De Vita *et al.* 2019). Additionally, the interface deformation is also found to be important for the gas–liquid turbulent drag reduction (Van den Berg *et al.* 2005; van Gils *et al.* 2013; Spandan, Verzicco & Lohse 2017; Lohse 2018; Mathai *et al.* 2020). The bubbles with large size or high deformability exhibit pronounced drag reduction effect (Lu, Fernández & Tryggvason 2005; Verschoof *et al.* 2016), but the drag reduction effect is lost when the bubbles are reduced to small sizes after the addition of surfactants (Verschoof *et al.* 2016).

Existing studies show that interface dynamics induce very different drag modulation effects in liquid–liquid and gas–liquid two-phase flows (Lohse 2018; Mathai *et al.* 2020; Yi *et al.* 2023). However, the role played by the fluid properties of the dispersed phase in these effects remains unclear. The interface dynamics, density and viscosity of the dispersed phase are intricately coupled, making it challenging to isolate the influence of the individual effects on drag modulation. In this study, we utilize interface-resolved three-dimensional direct numerical simulations to track interface dynamics in Taylor–Couette turbulence. Additionally, we employ momentum budget analysis to investigate the individual and coupling effects of the interface dynamics, density and viscosity of the dispersed phase. We aim to uncover how these factors operate and determine whether they cooperate or compete with each other in drag modulation.

2. Results and discussion

The interface-resolved three-dimensional direct numerical simulations of two-phase fluid–fluid flow in a Taylor–Couette (TC) system were carried out using a volume-of-fluid (VOF) method with the piecewise linear interface calculation (PLIC) based on the open-source OpenFOAM v8 (Rusche 2003; Chen, Zhao & Wan 2022). We consider two immiscible and incompressible fluids confined between two coaxial cylinders whose radii are r_i (inner) and r_o (outer). In this work, we have chosen to fix the outer cylinder while allowing the inner cylinder to rotate with a constant angular velocity ω_i. The two-phase flow is governed by the Navier–Stokes equations

$$\partial_t \rho + \nabla \cdot (\rho \boldsymbol{u}) = 0, \tag{2.1}$$

$$\partial_t (\rho \boldsymbol{u}) + \nabla \cdot (\rho \boldsymbol{u}\boldsymbol{u}) = -\nabla p + \nabla \cdot [\mu(\nabla \boldsymbol{u} + \nabla^{\mathrm{T}} \boldsymbol{u})] + \boldsymbol{f}, \tag{2.2}$$

where $\boldsymbol{u}$ is the velocity and p is the pressure. The ρ and μ are the variable density and viscosity, respectively. The continuous carrier phase is characterized by the density ρ_f and viscosity μ_f, whereas the dispersed phase is described by the density ρ_d and viscosity μ_d. The phase fraction α is introduced to characterize the variable density and viscosity, i.e. $\rho = \alpha\rho_d + (1-\alpha)\rho_f$ and $\mu = \alpha\mu_d + (1-\alpha)\mu_f$. The continuum surface force method, as proposed by Brackbill, Kothe & Zemach (1992), is adopted in this study to describe the interfacial tension, i.e. $\boldsymbol{f} = -\sigma\kappa\nabla\alpha$, where σ denotes the surface tension coefficient and $\kappa = \nabla \cdot (\nabla\alpha/|\nabla\alpha|)$ represents the interface curvature. The accuracy of the VOF method is often affected by interface sharpness (Gamet *et al.* 2020) and spurious currents (Vachaparambil & Einarsrud 2019; Fan & Anglart 2020). The detailed numerical methods and computational accuracy are presented in the supplementary material available at https://doi.org/10.1017/jfm.2024.206.

In the simulated TC system, a rotational symmetry of six (i.e. the simulated azimuthal region is set as $\pi/3$) is chosen to reduce computational costs without compromising the accuracy of our results. This choice has been validated for both single phase and multiphase TC turbulence (Brauckmann & Eckhardt 2013; Spandan, Verzicco & Lohse 2018; Assen *et al.* 2022; Xu *et al.* 2022, 2023). The curvature of a TC system is defined as $\eta = r_i/r_o = 0.714$ and the aspect ratio is defined as $\Gamma = L/d = 2\pi/3$, where $d = r_o - r_i$ is the gap width and L is the axial length. No-slip and impermeable boundary conditions are imposed in the radial direction, while periodicity is imposed in the axial and azimuthal directions. The inner and outer cylinders are subjected to a Neumann boundary condition for the phase fraction, resulting in a default contact angle of 90°. The system is uniformly discretized by (336 × 192 × 192) grid points in the azimuthal, radial and axial directions, respectively. The grid spacing is measured in wall units y^+ based on the shear stress at the inner cylinder for single-phase flow. In the radial direction, the uniform grid spacing is $0.725y^+$. Alternatively, a total amount of six grids is embedded inside the viscous sublayer, whose thickness is $0.0359d$. The uniform grid spacing in the axial direction is $1.519y^+$. The grid spacing in the azimuthal direction ranges from $1.085y^+$ near the inner wall to $1.519y^+$ near the outer wall. The Reynolds number $Re = \rho_f r_i \omega_i d/\mu_f$ and the Weber number $We = \rho_f r_i^2 \omega_i^2 d/\sigma$ are fixed at 2000 and 1260, respectively. The Taylor number is fixed as $Ta = [Re(1+\eta)^3/(8\eta^2)]^2 = 6.1 \times 10^6$. Due to the increased computational resources required for resolving the two-phase interface and the smaller time step needed to capture capillary wave propagation (Brackbill *et al.* 1992) in the two-phase flow compared with the single-phase case, we have chosen $Ta = 6.1 \times 10^6$ to ensure compatibility with our available computational resources. When the Taylor number exceeds 3×10^6, the flow field transitions into the classical regime of TC turbulence (Grossmann, Lohse & Sun 2016). Our chosen Taylor number falls within this regime, ensuring an adequate amount of turbulence information. The Weber number of 1260 is chosen to ensure that the spurious velocities remain within an acceptable range, as depicted in figure S2 in the supplementary material. The maximum Courant–Friedrichs–Lewy number is set to be 0.2. All the presented statistics are collected for at least 20 turns over time after reaching a statistically steady state.

Due to the centrifugal effect in the TC system, the distribution of dispersed phase is affected by the density ratio $\xi_\rho = \rho_d/\rho_f$ as well as the viscosity ratio $\xi_\mu = \mu_d/\mu_f$ of the dispersed phase to the continuous phase. Figure 1 displays the instantaneous interface snapshots and phase distribution for the dispersed phase volume fraction of $\varphi = 20\,\%$,

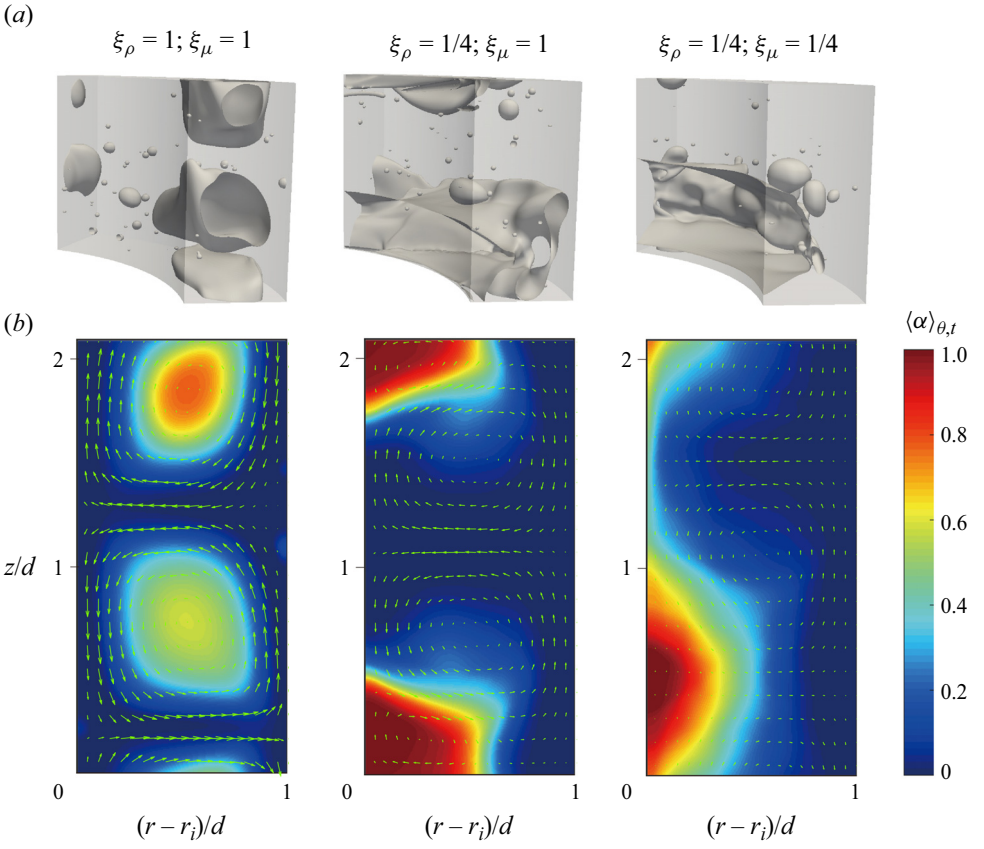

Figure 1. Instantaneous interface snapshots and corresponding azimuthally and time-averaged phase fraction $\langle\alpha\rangle_{\theta,t}$. The green arrows indicate the direction and magnitude of the averaged radial–axial velocity vectors $\langle u_{rz}\rangle_{\theta,t}/u_i$, where $u_i = \omega_i r_i$ is the velocity of the inner cylinder and z denotes the axial position.

providing valuable insights into the spatial distribution and behaviour of the interface and phase components in the system. The averaged radial–axial velocity vectors are also displayed by green arrows to denote the structure and strength of the Taylor vortex. When $\xi_\rho = 1$ and $\xi_\mu = 1$, the dispersed phase predominantly accumulates at the centre of the Taylor vortex, which is primarily attributed to the linear shear gradient present in the system (Hori *et al.* 2023). When $\xi_\rho = 1/4$ and $\xi_\mu = 1$, the dispersed phase migrates towards the inner wall of the system due to the centrifugal force exerted by the rotating flow. Consequently, the dispersed phase gathers in the plume ejection region near the inner wall and weakens the Taylor vortex. Furthermore, when $\xi_\rho = 1/4$ and $\xi_\mu = 1/4$, the distribution of the dispersed phase becomes more concentrated near the inner wall and the Taylor vortex is again weakened. The results indicate that decreasing the density ratio ξ_ρ and the viscosity ratio ξ_μ facilitates the gathering of the dispersed phase near the inner wall and the weakening of the Taylor vortex. Our objective is to analyse the specific effects of dispersed phase density and viscosity on the process of drag reduction.

Through sequential variations of the volume fraction φ, the density ratio ξ_ρ and the viscosity ratio ξ_μ, we conducted a comprehensive study to investigate the influence of these parameters on the drag modulation (see table 1). The results reveal several important findings. Firstly, when $\xi_\rho = 1$ and $\xi_\mu = 1$, it causes a minor increase in drag, indicating

φ	$\xi_\rho = \rho_d/\rho_f$	$\xi_\mu = \mu_d/\mu_f$	Drag modulation $((T/T_{\varphi=0}) - 1)$
0	—	—	—
10 %	1	1	+0.63 %
10 %	1/4	1	−16.02 %
10 %	1/4	1/4	−23.44 %
20 %	1	1	+1.04 %
20 %	1/4	1	−28.31 %
20 %	1/4	1/4	−50.23 %

Table 1. Drag modulation in two-phase flow. Here T represents the torque exerted on the inner cylinder and $T_{\varphi=0}$ denotes the torque specifically associated with the single-phase flow condition.

a slight drag enhancement effect. However, when we lower ξ_ρ to 1/4, a significant drag reduction is observed. Moreover, further reducing ξ_μ to 1/4 enhances the drag reduction effect even more. Furthermore, we found that the drag modulation shows similar trends for the dispersed phase volume fraction of $\varphi = 10\,\%$ and $\varphi = 20\,\%$. Under fixed density ratio ξ_ρ and viscosity ratio ξ_μ, an increase in the volume fraction φ leads to a stronger drag enhancement or drag reduction effect. In other words, as the volume fraction of the dispersed phase increases, the influence on the drag becomes more pronounced. These results highlight the significant impact of the dispersed phase's density, viscosity and volume fraction on the flow dynamics, particularly in terms of drag enhancement and drag reduction effects.

Given the similar trends in drag modulation for the dispersed phase volume fraction of $\varphi = 10\,\%$ and $\varphi = 20\,\%$, we next focus on the case with $\varphi = 20\,\%$. To investigate the impact of the dispersed phase on the flow field, figure 2 displays the radial profiles of the normalized azimuthal momentum and pressure calculated based on the phase distribution (see the inset figure) as a reference. When $\xi_\rho = 1$ and $\xi_\mu = 1$, the azimuthal momentum in the bulk region of the two-phase flow shows a slight decrease. The pressure is modulated in the region away from the inner cylinder and shows a decrease near the outer cylinder. Specifically, the modulation starts at a point where the phase fraction deviates from zero, but the modulation is insignificant overall. By reducing the density ratio ξ_ρ or viscosity ratio ξ_μ, a notable decrease in the azimuthal momentum and pressure in the bulk region is observed, aligning with the observed drag modulation. It is revealed that the reduction in the density ratio and the viscosity ratio plays a vital role in causing this decrease. The density ratio and the viscosity ratio are identified as key factors influencing drag reduction.

To investigate the effects of dispersed phase density and viscosity on the turbulent transport, we investigate the radial profile of total shear stress (figure 3*a*), viscous shear stress (figure 3*b*) and their difference (figure 3*c*). Due to the density difference between the dispersed and continuous phases, the Reynolds averaging is no longer applicable. We therefore adopt the Favre averaging (Favre 1969), which applies a density-weighted average to the velocity. The difference between the total shear stress and viscous shear stress is thus written as $\tau - \tau_\mu = -\langle \rho u_\theta'' u_r'' \rangle_{A,t}$ (hereafter referred to as Favre shear stress), which could be used to characterize the turbulence term. For the two-phase flow with $\xi_\rho = 1$ and $\xi_\mu = 1$, the profiles of the shear stresses are nearly identical to those for the single-phase case. However, by reducing the density ratio ξ_ρ or viscosity ratio ξ_μ, a significant decrease in the total shear stress is observed due to the decrease near the wall for the viscous shear stress and the decrease in the bulk region for the Favre shear stress, which is consistent with the observed drag reduction.

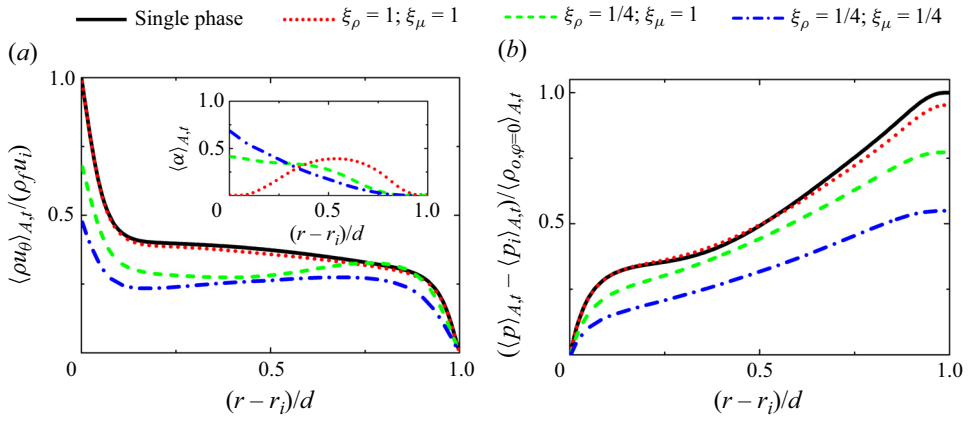

Figure 2. (*a*) The azimuthal momentum $\langle \rho u_\theta \rangle_{A,t}/(\rho_f u_i)$ and (*b*) pressure $(\langle p \rangle_{A,t} - \langle p_i \rangle_{A,t})/\langle p_{o,\varphi=0} \rangle_{A,t}$ as a function of the radial position, where u_θ is the azimuthal velocity, p_i is the pressure at the inner cylinder, and $p_{o,\varphi=0}$ is the pressure at the outer cylinder in single-phase flow. Correspondingly, the inset figure exhibits the radial profile of phase fraction $\langle \alpha \rangle_{A,t}$. The average operator $\langle \cdot \rangle_{A,t}$ is to obtain the axially, azimuthally and time-averaged value of the quantity.

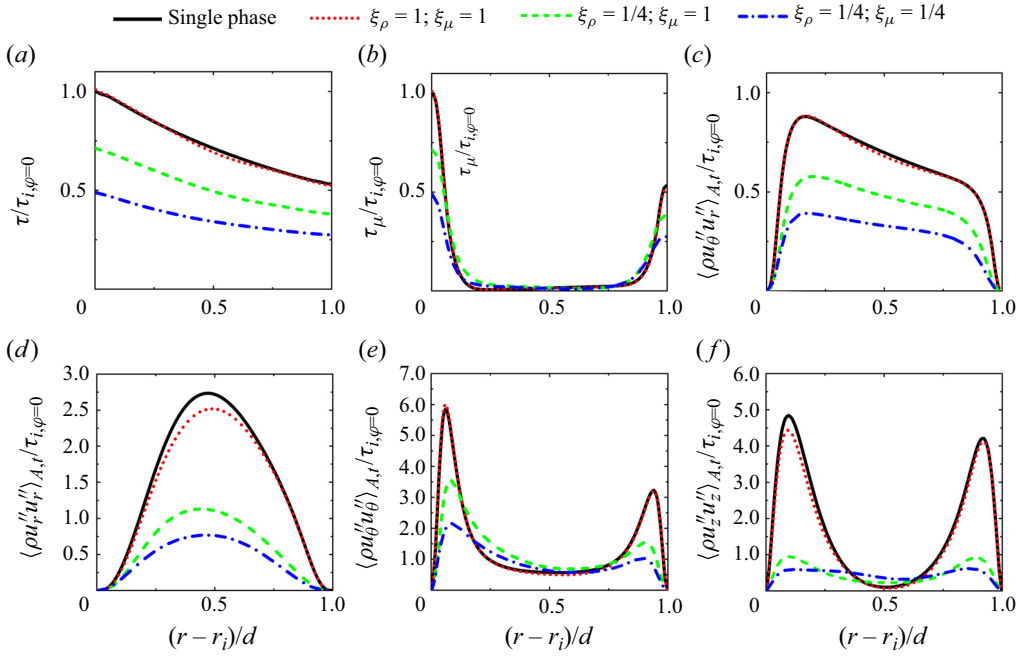

Figure 3. (*a*) The total shear stress $\tau/\tau_{i,\varphi=0}$, (*b*) viscous shear stress $\tau_\mu/\tau_{i,\varphi=0}$ and (*c*) Favre shear stress $-\langle \rho u_\theta'' u_r'' \rangle_{A,t}/\tau_{i,\varphi=0}$ as a function of the radial position, where $\tau_{i,\varphi=0}$ is the total shear stress on the inner cylinder in single-phase flow. The Favre normal stresses (*d*) $\langle \rho u_r'' u_r'' \rangle_{A,t}/\tau_{i,\varphi=0}$, (*e*) $\langle \rho u_\theta'' u_\theta'' \rangle_{A,t}/\tau_{i,\varphi=0}$, and (*f*) $\langle \rho u_z'' u_z'' \rangle_{A,t}/\tau_{i,\varphi=0}$ are also shown as a function of the radial position, where $u_r'' = u_r - \langle \rho u_r \rangle_{A,t}/\langle \rho \rangle_{A,t}$, $u_\theta'' = u_\theta - \langle \rho u_\theta \rangle_{A,t}/\langle \rho \rangle_{A,t}$ and $u_z'' = u_z - \langle \rho u_z \rangle_{A,t}/\langle \rho \rangle_{A,t}$ are the fluctuations of radial velocity u_r, azimuthal velocity u_θ and azimuthal velocity u_z, respectively.

To further study the influence of the dispersed phase on the turbulence fluctuations, we show the Favre normal stresses (figure 3*d–f*), which are generally investigated by the root mean square (r.m.s.) velocity fluctuations in the constant density flow system (Zhu *et al.* 2016; Wang *et al.* 2023*b*). For the two-phase flow with $\xi_\rho = 1$ and $\xi_\mu = 1$, the normal stress modulation is not very significant and the profiles of the normal stresses almost coincide with those for the single-phase case. By reducing the density ratio ξ_ρ or viscosity ratio ξ_μ, there is an overall reduction in the normal stress $\langle \rho u_r'' u_r'' \rangle_{A,t}$. The normal stress $\langle \rho u_\theta'' u_\theta'' \rangle_{A,t}$ shows a significant decrease near the inner and outer cylinders, while an increase is seen in the bulk region. A similar phenomenon has also been found in the study of the r.m.s. streamwise velocity fluctuations for polymer drag reduction systems, i.e. the r.m.s. streamwise velocity fluctuations decrease near the wall but increase away from the wall (Min *et al.* 2003; Wang *et al.* 2023*b*). The normal stress $\langle \rho u_z'' u_z'' \rangle_{A,t}$ shows a stronger reduction, indicating that the Taylor vortex has been significantly weakened as indicated by the averaged radial–axial velocity vectors in figure 1. As a result, the drag reduction caused by decreasing the density or viscosity of the dispersed phase is accompanied by a significant decrease in turbulence fluctuations.

To quantitatively characterize the effect of dispersed phase density and viscosity in drag modulation, we have derived a conserved quantity J^ω that characterizes the radial transport of azimuthal momentum in the two-phase TC turbulence,

$$J^\omega = J^\omega_{adv}(r) + J^\omega_{dif}(r) + J^\omega_{int}(r), \tag{2.3}$$

and provided the explicit expressions for the three terms on the right-hand side of (2.3), which are contributions from advection, diffusion and two-phase interface, respectively (see supplementary material for the detailed derivations):

$$J^\omega_{adv}(r) = \langle r^3 \rho u_r \omega \rangle_{A,t}, \tag{2.4}$$

$$J^\omega_{dif}(r) = -\langle \mu (r^3 \partial_r \omega + r \partial_\theta u_r) \rangle_{A,t}, \tag{2.5}$$

$$J^\omega_{int}(r) = -\int_r \langle r^2 f_\theta \rangle_{A,t} \, \mathrm{d}r. \tag{2.6}$$

These three terms are closely related to density, viscosity and interfacial tension, respectively. By normalizing (2.3) with the single-phase non-vortical laminar current $J^\omega_{lam} = 2\mu_f r_i^2 r_o^2 \omega_i / (r_o^2 - r_i^2)$, we obtain the Nusselt number $Nu_\omega = J^\omega / J^\omega_{lam}$, which represents the overall transport of azimuthal momentum. Additionally, we can express the contributions of advection ($Nu_{\omega,adv}(r)$), diffusion ($Nu_{\omega,dif}(r)$) and two-phase interface ($Nu_{\omega,int}(r)$) as functions of the radial position r. It is well-established that the Nusselt number Nu_ω and torque T in the TC system are related through the equation $T = 2\pi L J^\omega_{lam} Nu_\omega$ (Eckhardt, Grossmann & Lohse 2007). This relationship offers a convenient way to effectively decouple the effects of density, viscosity and two-phase interface on drag reduction (see figure S3 in the supplementary material). Note that the advection contribution comprises both an average part and a turbulent part, with the average part being negligible compared with the turbulent part (see figure S4 in the supplementary material). Therefore, similar to that in plate flows (Picano, Breugem & Brandt 2015; Wang, Jiang & Sun 2023*a*), the advection contribution may be equivalent to the turbulence contribution.

For the two-phase flow with $\xi_\rho = 1$ and $\xi_\mu = 1$, the advection contribution is slightly reduced in regions where the interface contribution is relatively large (see figure 4*a*,*c*), suggesting that the two-phase interface has a subtle modulation effect on the advection processes, consistent with the conservation of azimuthal momentum transport.

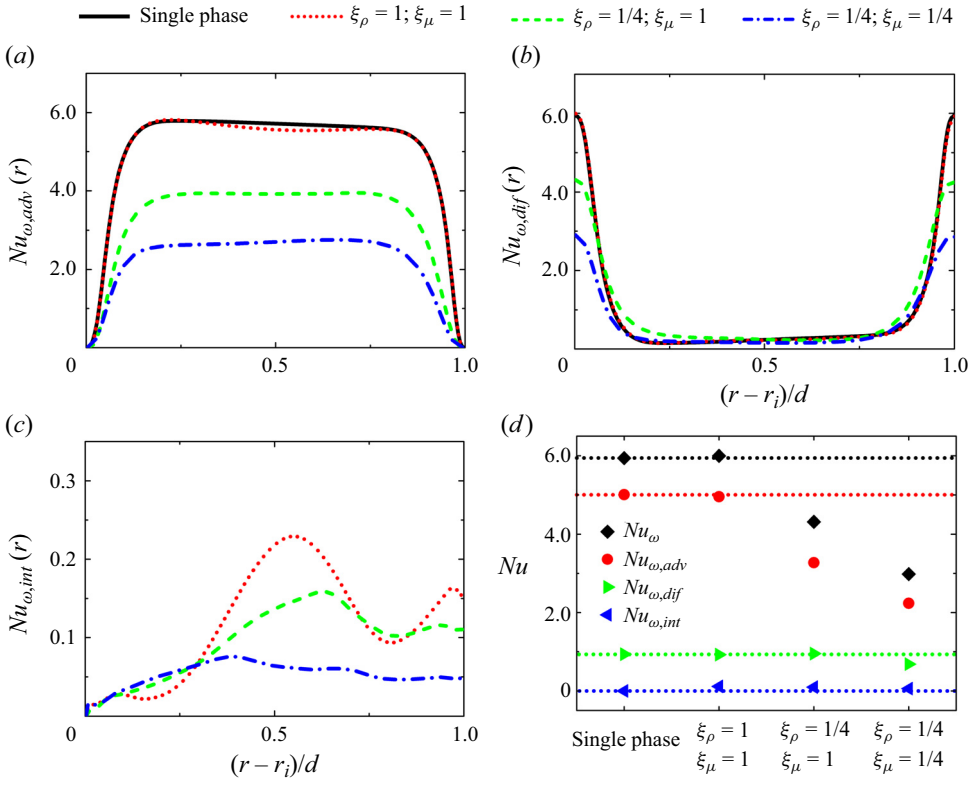

Figure 4. Momentum transport analysis. (*a*) The normalized advection contribution, (*b*) the normalized diffusion contribution and (*c*) the normalized interface contribution as a function of the radial position are shown. (*d*) The momentum transport and its three contributions are averaged in the radial direction to characterize the corresponding terms within the whole system. The dashed lines in (*d*) represent the averaged values for single-phase flow.

Considering the limited change in the diffusion contribution (see figure 4*b*), it is evident that the two-phase interface becomes the primary factor responsible for drag enhancement. In view of the insignificant effect of drag enhancement (see figure 4*d*), we additionally calculated a case where the Reynolds number and the surface tension coefficient are tripled, again showing the dominant role of interfacial tension in drag enhancement (see figure S5 in the supplementary material). It is important to note that the interface contribution, as shown in figures 4(*c*) and 4(*d*), is consistently positive, indicating that the two-phase interface does not contribute to drag reduction in the system. However, due to the small magnitude of the obtained interface contribution, which accounts for approximately 4 % of the conserved quantity, a more in-depth investigation specifically on this term should be conducted in future work.

Since the interface contribution ($J^{\omega}_{int}(r)$) acts primarily to increase drag and is very small in our drag reduction cases (see figure 4*d*), we will focus on the advection ($J^{\omega}_{adv}(r)$) and diffusion ($J^{\omega}_{dif}(r)$) contributions in the subsequent analysis. Lowering ξ_ρ to 1/4 results in a reduction in the local advection contribution. The density ratio $\xi_\rho = 1/4$ promotes dispersed phase's gathering near the inner wall, which in turn leads to a significant decrease in the upstream advection contribution. This ultimately results in an overall reduction in the advection contribution (see figure 4*a*). Based on the conservation

of momentum transport, the diffusion contribution is redistributed (see figure 4*b*) but the total diffusion contribution remains the same (see figure 4*d*). Further reducing ξ_μ to 1/4 causes a decrease in the local diffusion contribution near the inner wall (see figure 4*b*), ultimately leading to a reduction in the total diffusion contribution (see figure 4*d*). Additionally, based on the conservation of momentum transport, the advection contribution is modulated and again overall reduced (see figure 4*a*). It is evident that the combination of decreasing density ratio ξ_ρ and viscosity ratio ξ_μ plays a dominant role in drag reduction. Therefore, the blocking effect of the dispersed phase on momentum transport is due to the decreased density and viscosity ratios. In our ongoing preliminary simulations on drag modulation in two-phase plane-Couette turbulence, we have observed similar drag modulation mechanisms. This is beyond the scope of the current work and will be systematically investigated and compared with the present study in our future work.

Given the generality of (2.3), our conclusion can be extended to analyse bubble drag reduction in turbulent flows (van Gils *et al.* 2013). Due to the extremely low density and viscosity ratios of the bubble to the continuous phase, the advection and diffusion contributions are significantly reduced, resulting in drag reduction. Meanwhile, it has been reported that bubbly drag reduction is effective when large bubbles are present, but the drag reduction effect is lost when the bubbles are reduced to small sizes after the addition of surfactants (Verschoof *et al.* 2016). We can provide a physical understanding of this observation. When surfactants are added to decrease the surface tension coefficient, it leads to a reduction in bubble size. However, this reduction in bubble size is accompanied by an increase in the interfacial area in the system. As a result, the interface contribution to drag, which is enhanced by the increased interfacial area, offsets the drag reduction caused by the low density and viscosity ratios. Furthermore, the decrease in bubble size also attenuates the effective centripetal Froude number exerted on the small bubbles (van Gils *et al.* 2013), leading to a reduced accumulation of gas near the inner wall. This can explain why the drag reduction is lost when the bubbles are shrunk to small sizes after the addition of surfactants.

3. Conclusions

In conclusion, we have derived a conserved quantity that characterizes the radial transport of azimuthal momentum in fluid–fluid two-phase TC turbulence. This conserved quantity consists of three terms: the density-related advection contribution, the viscosity-related diffusion contribution and the interface contribution. Our analysis highlights the significant roles played by two-phase interface, density and viscosity ratios in modulating drag. Specifically, decreasing the density ratio of the dispersed phase to the continuous phase reduces the local advection contribution, while decreasing the viscosity ratio reduces the local diffusion contribution. Through modulation and redistribution, these effects lead to an overall reduction in momentum transport. On the other hand, the two-phase interface consistently produces a positive contribution to drag enhancement. By considering the interplay between density ratio, viscosity ratio and two-phase interface, we conclude that drag modulation is achieved through the combined influence of these factors. The current findings contribute to a better understanding of the mechanisms underlying drag reduction in two-phase turbulent flows.

Supplementary material. Supplementary material is available at https://doi.org/10.1017/jfm.2024.206.

Funding. This work is financially supported by the National Natural Science Foundation of China under grant no. 11988102 and the New Cornerstone Science Foundation through the New Cornerstone Investigator Program and the XPLORER PRIZE.

Declaration of interests. The authors report no conflict of interest.

Author ORCIDs.
Jinghong Su https://orcid.org/0000-0003-1104-6015;
Lei Yi https://orcid.org/0000-0002-0247-4600;
Bidan Zhao https://orcid.org/0000-0003-3390-1801;
Cheng Wang https://orcid.org/0000-0002-6470-7289;
Fan Xu https://orcid.org/0009-0004-3324-7859;
Junwu Wang https://orcid.org/0000-0003-3988-1477;
Chao Sun https://orcid.org/0000-0002-0930-6343.

References

Assen, M.P.A., Ng, C.S., Will, J.B., Stevens, R.J.A.M., Lohse, D. & Verzicco, R. 2022 Strong alignment of prolate ellipsoids in Taylor–Couette flow. *J. Fluid Mech.* **935**, A7.

Balachandar, S. & Eaton, J.K. 2010 Turbulent dispersed multiphase flow. *Annu. Rev. Fluid Mech.* **42**, 111–133.

Brackbill, J.U., Kothe, D.B. & Zemach, C. 1992 A continuum method for modeling surface tension. *J. Comput. Phys.* **100** (2), 335–354.

Brauckmann, H.J. & Eckhardt, B. 2013 Direct numerical simulations of local and global torque in Taylor–Couette flow up to $Re = 30\,000$. *J. Fluid Mech.* **718**, 398–427.

Cannon, I., Izbassarov, D., Tammisola, O., Brandt, L. & Rosti, M.E. 2021 The effect of droplet coalescence on drag in turbulent channel flows. *Phys. Fluids* **33** (8), 085112.

Ceccio, S.L. 2010 Friction drag reduction of external flows with bubble and gas injection. *Annu. Rev. Fluid Mech.* **42**, 183–203.

Chen, S., Zhao, W. & Wan, D. 2022 Turbulent structures and characteristics of flows past a vertical surface-piercing finite circular cylinder. *Phys. Fluids* **34** (1), 015115.

De Vita, F., Rosti, M.E., Caserta, S. & Brandt, L. 2019 On the effect of coalescence on the rheology of emulsions. *J. Fluid Mech.* **880**, 969–991.

Eckhardt, B., Grossmann, S. & Lohse, D. 2007 Torque scaling in turbulent Taylor–Couette flow between independently rotating cylinders. *J. Fluid Mech.* **581**, 221–250.

Fan, W. & Anglart, H. 2020 varrhoturbvof: a new set of volume of fluid solvers for turbulent isothermal multiphase flows in openfoam. *Comput. Phys. Commun.* **247**, 106876.

Favre, A. 1969 Statistical equations of turbulent gases. In *Problems of Hydrodynamics and Continuum Mechanics*, pp. 231–266. SIAM.

Gamet, L., Scala, M., Roenby, J., Scheufler, H. & Pierson, J.-L. 2020 Validation of volume-of-fluid OpenFOAM® isoAdvector solvers using single bubble benchmarks. *Comput. Fluids* **213**, 104722.

van Gils, D.P.M., Guzman, D.N., Sun, C. & Lohse, D. 2013 The importance of bubble deformability for strong drag reduction in bubbly turbulent Taylor–Couette flow. *J. Fluid Mech.* **722**, 317–347.

Grossmann, S., Lohse, D. & Sun, C. 2016 High–Reynolds number Taylor–Couette turbulence. *Annu. Rev. Fluid Mech.* **48**, 53–80.

Hakansson, A., Crialesi-Esposito, M., Nilsson, L. & Brandt, L. 2022 A criterion for when an emulsion drop undergoing turbulent deformation has reached a critically deformed state. *Colloids Surf.* A **648**, 129213.

Hori, N., Ng, C.S., Lohse, D. & Verzicco, R. 2023 Interfacial-dominated torque response in liquid–liquid Taylor–Couette flows. *J. Fluid Mech.* **956**, A15.

Kavehpour, H.P. 2015 Coalescence of drops. *Annu. Rev. Fluid Mech.* **47**, 245–268.

Lemenand, T., Della Valle, D., Dupont, P. & Peerhossaini, H. 2017 Turbulent spectrum model for drop-breakup mechanisms in an inhomogeneous turbulent flow. *Chem. Engng Sci.* **158**, 41–49.

Lohse, D. 2018 Bubble puzzles: from fundamentals to applications. *Phys. Rev. Fluids* **3** (11), 110504.

Lu, J., Fernández, A. & Tryggvason, G. 2005 The effect of bubbles on the wall drag in a turbulent channel flow. *Phys. Fluids* **17** (9), 095102.

Mathai, V., Lohse, D. & Sun, C. 2020 Bubbly and buoyant particle-laden turbulent flows. *Annu. Rev. Condens. Matter Phys.* **11**, 529–559.

Min, T., Yoo, J.Y., Choi, H. & Joseph, D.D. 2003 Drag reduction by polymer additives in a turbulent channel flow. *J. Fluid Mech.* **486**, 213–238.

Ni, R. 2024 Deformation and breakup of bubbles and drops in turbulence. *Annu. Rev. Fluid Mech.* **56**, 319–347.

OLAD, P., INNINGS, F., CRIALESI-ESPOSITO, M., BRANDT, L. & HAKANSSON, A. 2023 Comparison of turbulent drop breakup in an emulsification device and homogeneous isotropic turbulence: insights from numerical experiments. *Colloids Surf.* A **657**, 130569.

PICANO, F., BREUGEM, W.-P. & BRANDT, L. 2015 Turbulent channel flow of dense suspensions of neutrally buoyant spheres. *J. Fluid Mech.* **764**, 463–487.

RALLISON, J.M. 1984 The deformation of small viscous drops and bubbles in shear flows. *Annu. Rev. Fluid Mech.* **16** (1), 45–66.

ROSTI, M.E., DE VITA, F. & BRANDT, L. 2019 Numerical simulations of emulsions in shear flows. *Acta Mechanica* **230** (2), 667–682.

RUSCHE, H. 2003 Computational fluid dynamics of dispersed two-phase flows at high phase fractions. PhD thesis, Imperial College London (University of London).

SPANDAN, V., VERZICCO, R. & LOHSE, D. 2017 Deformable ellipsoidal bubbles in Taylor–Couette flow with enhanced Euler–Lagrangian tracking. *Phys. Rev. Fluids* **2** (10), 104304.

SPANDAN, V., VERZICCO, R. & LOHSE, D. 2018 Physical mechanisms governing drag reduction in turbulent Taylor–Couette flow with finite-size deformable bubbles. *J. Fluid Mech.* **849**, R3.

STONE, H.A. 1994 Dynamics of drop deformation and breakup in viscous fluids. *Annu. Rev. Fluid Mech.* **26** (1), 65–102.

VACHAPARAMBIL, K.J. & EINARSRUD, K.E. 2019 Comparison of surface tension models for the volume of fluid method. *Processes* **7** (8), 542.

VAN DEN BERG, T.H., LUTHER, S., LATHROP, D.P. & LOHSE, D. 2005 Drag reduction in bubbly Taylor–Couette turbulence. *Phys. Rev. Lett.* **94** (4), 044501.

VERSCHOOF, R.A., VAN DER VEEN, R.C.A., SUN, C. & LOHSE, D. 2016 Bubble drag reduction requires large bubbles. *Phys. Rev. Lett.* **117** (10), 104502.

WANG, C., JIANG, L. & SUN, C. 2023*a* Numerical study on turbulence modulation of finite-size particles in plane-Couette flow. *J. Fluid Mech.* **970**, A7.

WANG, S., ZHANG, W., WANG, X., LI, X., ZHANG, H. & LI, F. 2023*b* Maximum drag reduction state of viscoelastic turbulent channel flow: marginal inertial turbulence or elasto-inertial turbulence. *J. Fluid Mech.* **960**, A12.

XU, F., SU, J., LAN, B., ZHAO, P., HE, Y., SUN, C. & WANG, J. 2023 Direct numerical simulation of Taylor–Couette flow with vertical asymmetric rough walls. *J. Fluid Mech.* **975**, A30.

XU, F., ZHAO, P., SUN, C., HE, Y. & WANG, J. 2022 Direct numerical simulation of Taylor–Couette flow: regime-dependent role of axial walls. *Chem. Engng Sci.* **263**, 118075.

YI, L., TOSCHI, F. & SUN, C. 2021 Global and local statistics in turbulent emulsions. *J. Fluid Mech.* **912**, A13.

YI, L., WANG, C., HUISMAN, S.G. & SUN, C. 2023 Recent developments of turbulent emulsions in Taylor–Couette flow. *Phil. Trans. R. Soc.* A **381** (2243), 20220129.

YI, L., WANG, C., VAN VUREN, T., LOHSE, D., RISSO, F., TOSCHI, F. & SUN, C. 2022 Physical mechanisms for droplet size and effective viscosity asymmetries in turbulent emulsions. *J. Fluid Mech.* **951**, A39.

ZHU, X., OSTILLA-MÓNICO, R., VERZICCO, R. & LOHSE, D. 2016 Direct numerical simulation of Taylor–Couette flow with grooved walls: torque scaling and flow structure. *J. Fluid Mech.* **794**, 746–774.